Generating Antibacterial Microporous Structures Using Microfluidic Processing

Christina Katsakouli,[†,‡] Xinyue Jiang,[†] Wai Keith Lau,[†] Jennifer L. Rohn,[§] and Mohan Edirisinghe*[,†]
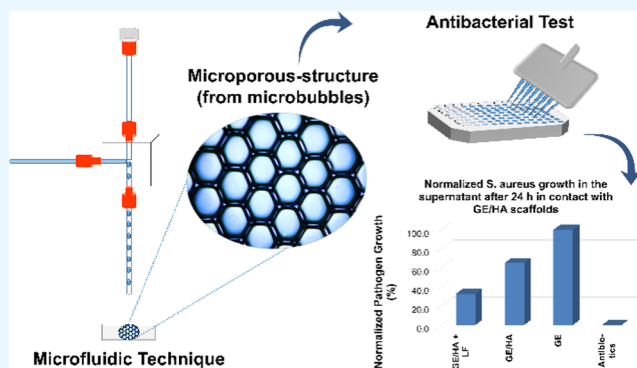
[†]Department of Mechanical Engineering, University College London, Torrington Place, WC1E 7JE London, U.K.
[‡]Faculty of Sport Sciences, Aix-Marseille University, 163 avenue de Luminy, 13009 Marseille, France
[§]Chronic UTI Group, Centre for Nephrology, University College London, WC1E 6BT London, U.K.

S Supporting Information

ABSTRACT: The aim of this study is to investigate the potential of microfluidic techniques to generate microporous structures, with potential utility as scaffolds, with a highly uniform architecture, possessing an antibacterial activity. Scaffolds were prepared by introducing N_2 gas to gelatin (GE)—water or gelatin/hyaluronic acid (GE/HA)—water mixtures to form microbubbles at the interface. The effect of solution temperature on microbubble stability and their structural integrity were studied. A solution temperature of 40 °C produced the best results due to the higher solution viscosity. The effect of different cross-linking concentrations on scaffold swelling ratio was investigated. A concentration of 5% glutaraldehyde was found to be optimal and was chosen to cross-link structure and conduct subsequent degradation and antibacterial experiments. HA was incorporated into the scaffolds owing to its ability to make stable and highly absorbent scaffolds. This led to a decrease in the degradation rate and the introduction of an antibacterial effect. This effect could be further enhanced with the inclusion of lactoferrin. This work is the first reported attempt for making antibacterial GE/HA scaffolds by using microfluidics.

INTRODUCTION

Recently, remarkable research has been conducted to develop bioactive scaffolds, which are analogous to the extracellular matrix (ECM), that have a significant impact in the field of tissue engineering, as their ideal ability to act as a conduit to guide cell growth and subsequent tissue formation.[1,2] The key challenge is to produce scaffolds which facilitate tissue—cell interactions while preventing bacterial colonization. Antibacterial scaffolds have been applied in a broad range of tissue engineering applications such as bone, cartilage, ligament, skin, vascular tissues, neural tissues, and bone tissues. Their porosity is the key factor in enhancing the transportation of nutrients and oxygen.[3] This has captured the attention of many researchers keen to develop more effective approaches for obtaining porous scaffolds with improved characteristics. Existing manufacturing techniques for porous scaffolds include gas forming, electrospinning, phase separation, freeze drying, and particulate leaching.[4] All these techniques introduce porosity since a porous surface not only allows the migration and proliferation of cells but also vascularization.[5] Scaffolds produced via these conventional technologies have a wide distribution of pore sizes or irregularities in their structures consequently resulting in difficulties during the conduct of systematic research aimed at investigating the effect of structure on the differences in signaling, gene expression, and organization. Also, using these conventional methods to produce scaffolds results in a lack of control over the structure and interconnectivity of scaffolds, furthermore affecting the mechanical properties.[6] Ordered and uniformed spatial structures are beneficial in the study of cell-to-cell and cell-to-matrix interactions. A uniform spatial structure also contributes to the homogeneous distribution of chemical stimuli.[7] In this study, the microfluidic technique is employed to fabricate scaffolds with a desirable homogenous porosity,[8] interconnectivity, and potential mechanical properties.[6] This process can be readily scaled up by incorporating multiple T-junction devices into the production method.[8] Wang et al.[9] showed that by collecting bubbles over a period of time, the fabrication of a sponge-type, multilayer scaffold was successful, which promoted more cell migration and distribution in the scaffold through chondrocyte proliferation. Ekemen et al.[10] used microbubbling to fabricate scaffolds for tissue engineering applications as their open pores are ideal for integration and cell proliferation.

Three key factors need to be considered in the design of ideal scaffolds intended to mimic the natural extracellular matrix (ECM) of a targeted tissue. These are the scaffolds' mechanical properties, structure, and biological signaling.[11]

Table 1. Material Properties of 5 w/w % GE at 40, 50, and 60 °C[a]

solution	temperature (°C)	viscosity (mPa s)	density (g/mL)	surface tension (mN/m)
5 w/w % GE/HW	40	25.27 ± 0.74	1.01 ± 0.02	54.6 ± 1.23
5 w/w % GE	40	19.85 ± 0.71	1.02 ± 0 03	43.52 ± 2.16
5 w/w % GE	50	5.66 ± 0.66*	1.06 ± 0.08	44.76 ± 0.03
5 w/w % GE	60	4.61 ± 0.43*	1.02 ± 0.007	41.74 ± 0.07

[a]Each measurement was repeated five times and values are expressed in mean ± standard error of the mean. One-way analysis of variance (ANOVA) was carried out followed by post hoc Tukey multiple comparison test. GE solutions (5 wt %) at three different temperature were compared and values are represented statistically when *$p < 0.05$ in comparison with 5 wt % GE in 40° solution. Statistical analysis was performed using the GraphPad Prism 6.0 software (GraphPad Software, Inc., San Diego, CA). There is no significant difference in density and surface tension between 5 wt % GE solutions at three different temperatures. The viscosity of 5 wt % GE solution at 40° is significantly higher ($p < 0.05$) compared to the other two solutions at 50 and 60 °C.

Natural ECM is comprised of a cross-linked porous structure of collagens embedded with glycosaminoglycans and proteins.[2,12] Currently, a large number of extracellular matrix-inspired protein and polysaccharide-based materials exist.[12] Among them, hyaluronic acid (HA) as a natural skin component is the most frequently used compound for soft tissue fillers. HA is a biocompatible, biodegradable natural material composed of approximately 10 000 repeat units of the disaccharide units of D-glucuronic acid and N-acetyl-D-glucosamine.[1,12] HA has many important roles in the body. These include the good maintenance of extracellular space, reinforcement of extracellular transportation of nutrients and ions, manipulation of hydration of tissues, and binding of interleukins and growth factors.[12−14] It has also been shown that HA interacting with proteins can facilitate natural ECM assembly under physiological conditions.[1,15] HA−protein hybrids can stabilize ECM and subsequently regulate cell adhesion and growth.[16] As a result, HA has been widely used as ideal scaffold materials for skin, cartilage, bone ligament, brain and nerve tissue engineering applications.[17−19] Despite this, HA is not thermodynamically conducive to cell attachment or tissue formation. These properties are a result of its polyanionic and highly hydrophilicity nature.[16,20] There are a few methodologies to address this challenge. One of the major approaches is to develop HA-based scaffolds in the presence of nanofibers, hydrogels, and sponges by integrating HA with biomaterials such as collagen, gelatin, chitosan, and silk fibroin.[1] HA has been chosen for this study as it has an antimicrobial response.[17,18,21]

Collagen is the major protein component of ECM. As GE is produced from collagen denaturation, it contains some of the collagen precursor chemotactic signals (RGD amino acid sequence, which can facilitate cell attachment). Thus, gelatin is considered a cost-effective replacement to collagen for the various potential applications in tissue engineering.[3] Gelatin is broadly used as a material in the fabrication of scaffolds for cartilage, bone, and nerve tissues.[17] Gelatin also has a good gas foaming ability and in this study was the major structural component which was used to blend with HA to fabricate GE/HA hybrid structures with potential use as scaffolds. The use of natural materials as well as high porosity are two factors which are implicated in bacterial growth as well as cell growth.

Lactoferrin (LF) is a glycoprotein and belongs to the transferrin family, delivered from human or bovine milk. Lactoferrin works as an opsonin to promote bacterial clearance.[21] LF binds the iron, resulting in sequestered iron, which is one of the most necessary nutritional requirements for most bacterial pathogens and thus inhibits the growth of a broad spectrum of bacterial strains.[21] It has been shown from previous studies that lactoferrin has (i) the ability to promote the proliferation and differentiation of osteoblasts, suggesting its potential utility as an osteogenic growth factor in bone tissue engineering,[22] (ii) multiple functions including immunomodulatory, anticancer, antibacterial, anti-inflammatory, and antiviral activities.[21,23] LF has been chosen for this study for its antibacterial activity and its nontoxic effects.[24−26]

In this study, antibacterial structures were generated to prevent and limit infections without the use of antibiotics as its long-term use can provoke toxic and adverse effects. The need for prevention of implant-associated bacterial infections has led this research to combine microfluidics with the fabrication of antibacterial scaffolds made from natural biomaterials. GE and HA were chosen as the scaffold materials to mimic the vital components of the ECM. The microfluidic technique was used to generate monodispersed microbubbles which were the precursors to the scaffolds. These scaffolds were cross-linked with glutaraldehyde (GA). The operating temperature, cross-linking concentrations, swelling ratio, and degradation were also studied in this work. Moreover, the potential to incorporate natural antibiotic agents into the scaffolds was investigated in vitro by testing against *Staphylococcus aureus*. *S. aureus* was chosen as a model bacteria for this study as it is a major cause of nosocomial-acquired infections and can not only provoke healthcare-associated infections such as ventilator-associated pneumonia, surgical site infection, and catheter-associated bloodstream infection but is also associated with community-onset infections such as skin and soft tissues infections.[27,28]

The aim of this study was to produce highly organized porous structures and assess their antibacterial activity, as no other study was found to have studied the antibacterial activity of microbubble scaffolds. Gelatin and hyaluronic acid have been used in several studies as scaffolding materials to mimic components of the ECM, but this study is the first that combines GE/HA with LF to create antibacterial scaffolds using microbubbles.

■ RESULTS AND DISCUSSION

Stability Test. GE microbubbles were generated using 5 w/w % GE solution heated to temperatures of 40, 50, or 60 °C and delivered with a constant liquid flow rate of 80 μL/min to the T-junction microfluidic device. Gas pressure was adjusted between 200 and 300 kPa to achieve approximately the same initial bubble size. The average initial bubble size made from these three solutions was 315 μm with a standard deviation of 7%. After processing, the scaffold pore size is proportional to the diameter of the initially generated microbubbles. The produced pore size is desirable as the pore size should be large
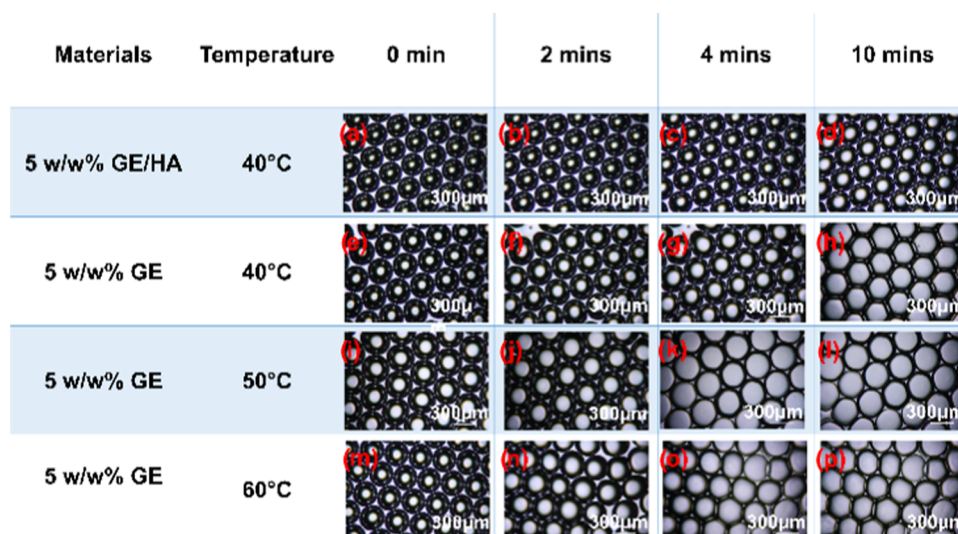
Figure 1. Structure of GE and GE/HA two-dimensional (2D) scaffolds, fabricated by microbubbles. From left to right, start point and after 2, 4, and 10 min (a–d) GE/HA at 40 °C, (e–h) GE at 40 °C, (i–l) GE at 50 °C, (m–p) GE at 60 °C water bath temperature, respectively.

enough to allow communication between cells, access to nutrition, and ECM formation. Murphy et al.[29] show that the cell proliferation was the highest in scaffolds with a pore size of 300 μm in comparison to smaller pore sizes, as cells can more easily attach to large surfaces.[30]

To study the effect of GE solution temperature on the stability of the resulting microbubbles and the structure of scaffolds produced by microbubbles after drying, material properties of 5 w/w % GE solutions at 40, 50, or 60 °C were measured (Table 1). Table 1 shows that amongst the three different temperatures, viscosity is the main parameter which has substantially changed. Solution viscosity decreased, as the water bath temperature was increased from 40 to 60 °C. The highest solution viscosity is 19.85 ± 0.71 mPa s at 40 °C. There is no significant difference in density and surface tension between 5 wt % GE solutions at three different temperatures with standard deviations of 0.01 and 1.5, respectively.

As demonstrated in Figure 1, the least stable microbubbles were produced by solutions at 60 °C (Figure 1i), where microbubbles started to dry out within 2 min without cross-linking. On the other hand, microbubbles generated at 40 °C (stable for up to 4 min without cross-linking) were observed to be the most stable (Figure 1e). The stability difference is most likely caused by the sharp viscosity contrast between 5 w/w % GE at 40 and 60 °C (Table 1). The difference in viscosity also contributes to the formation of scaffolds. Honeycomb-shaped scaffolds were created with solutions heated to 40 °C (Figure 1h). Conversely, scaffolds with irregularities were formed with solution heated up to 60 °C. This is a result of the lower shell viscosity of the microbubbles, which is insufficient to resist the distortion forces caused by solvent evaporation.[31] This is in agreement with previous reports that increasing the viscosity of the continuous phase can prolong the life span of the droplets surrounded by polymer.[6] This in turn reduces the number of defects which are evident in Figure 1m−p for solution at 60 °C and improves structure uniformity, Figure 1e−h. After the formation of GE microbubbles at 40 °C, GE/HA microbubbles were produced under the same conditions, proving that GE/HA microbubbles remain stable and uniform, and the resultant scaffolds retain a well-ordered honeycomb structure for a longer period of time than GE scaffolds, as shown in Figure

1c,d. The stability of the microbubbles after cross-linking was not studied in detail in this work, however, during the timespan of experimental degradation (~1 week), the bubbles were stable in phosphate-buffered saline (PBS) under 37 °C. Thus, the cross-linking helps to stabilize, i.e., retain both shape and size.

As illustrated in Figure 2, the smallest diameter (295 μm with a polydispersity index (PDI) of 0.01) microbubbles were
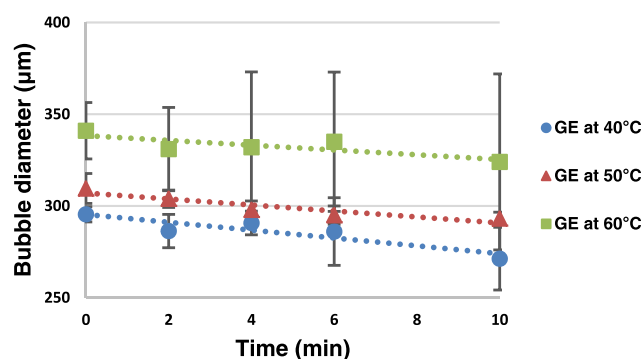

Figure 2. Effect of temperature on microbubble size at different temperatures, 40, 50, and 60 °C.

produced with solutions at 40 °C. The largest bubble diameter (341 μm with a PDI of 0.04) was created with solutions at 60 °C. Microbubbles shrink as a function of time as gas dissolves into the surrounding.[8] The reduction in size leads to increased stability (Figure 1). The stability of the microbubbles depends on several resistance parameters like gravitational drainage, Oswald's ripening, and Laplace pressure, where gas diffusion through the surrounding liquid shell is prompted by the pressure gradient (Laplace pressure).[32] This trend can be explained by the fact that microbubbles made at 40 °C had lower rates of gaseous diffusion into the liquid shell.[8] As the stability of microbubbles under ambient conditions is governed by their radius and Laplace pressure is inversely related to microbubble radius, smaller microbubbles have lower gas exchange rates.[8] Additionally, the resistance from their condensed hard shell to gas permeation is also a vital

contributor to the stability of gas-filled microbubbles.[33] The higher solution viscosity (19.85 ± 0.71 mPa s, Table 1) at 40 °C condensed the relevant shells of microbubbles. Hence, microbubbles produced at 40 °C are more stable, and the resultant scaffolds have well-ordered honeycomb structures. As a result, the temperature of the solution precursor affects the stability and quality of the microbubbles, due to the change in solution viscosity (Figure 1).

Effect of Solution Viscosity on Microbubble Diameter. As shown in Figure 3, dimensionless diameter of
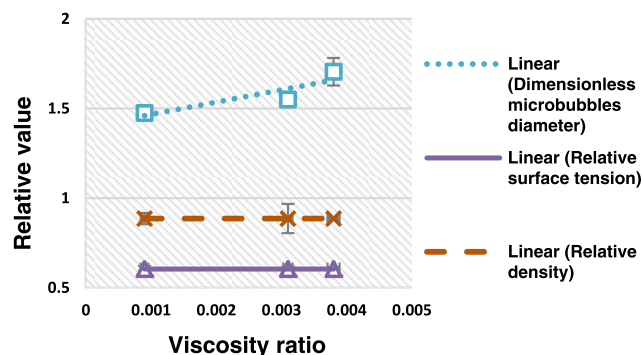

Figure 3. Relative value for 5 w/w % GE solution at 40, 50, and 60 °C of density, surface tension, and dimensionless microbubble diameter as a function of solution viscosity ratio.

microbubbles produced by cross-flow rupture technique corresponds to the solution viscosity ratio (Table 2) of the

Table 2. Effect of Solution Temperature on Viscosity Ratio of 5 w/w % GE, Where Viscosity Ratio Represents the Ratio of the Dispersed Phase (Nitrogen) to the Continuous Phase

temperature (°C)	40	50	60
viscosity ratio	0.0009	0.0031	0.0038

dispersed phase to that of the continuous phase. In other words, the diameter of microbubbles increased with decreasing continuous phase viscosity, where dimensionless microbubble diameter is the ratio of diameter of microbubbles to the size of channel (200 μm in Figure 1). However, the relative surface tension of 0.6 and relative density of 0.9 are kept constant and unaffected by the change of solution viscosity ratio, where the relative surface tension and density are expressed as the ratio of surface tension/density of dispersed phase to the surface tension/density of continuous phase, respectively. Thus, the relation between microbubble size and material properties can be seen from Figure 3 where microbubble sizes generated in the T-junction are decreased with increasing continuous phase viscosity and independent of material surface tension. This can be explained using the capillary number. There are several dimensionless parameters that reveal the formation of droplets and bubbles in microfluidic T-junctions. The key parameter among them is capillary number, which is the ratio of viscosity to interfacial tension.[8] The diameter of bubbles decreases with increasing capillary number.[34] Therefore, microbubbles with a nonsignificant surface tension deviation of 1% generated by solution at 60 °C are larger than the size of microbubbles produced at 40 °C.

Previous reports for gas−liquid systems observed that average bubble size increased with increasing viscosity of the continuous phase.[35,36] This apparent contradiction is due to

the different breakup mechanisms involved in different microfluidic techniques.[37] The formation of microbubbles in these reports[35,36] was achieved by geometry-dominated breakup, where the formation of microbubbles is dominated by the spontaneous transformation caused by surface tension.[35,37] However, in this paper, microbubbles were formed though the cross-flow rupture technique (T-junction). In this device, microbubble size is related to the flow rate ratio and phase viscosity.[36,37]

A well-structured scaffold is desirable as highly ordered and uniform spatial structures are beneficial for cell-to-cell and cell-to-matrix interactions.[7] As the 2D scaffold is well structured at 40 °C, 5 w/w % GE solution heated to 40 °C was chosen as the base solution for all the following experiments.

Swelling Behavior. The swelling ratio of scaffolds plays a vital role in maintaining the stability of the scaffold structure and its mechanical properties when implanted in vivo.[33] Hence, the swelling ratio is a key parameter to evaluate the structural stability of GE scaffolds. Cross-linking is a necessary step in preparing stable three-dimensional (3D) biopolymer scaffolds[18] as gelatin has poor mechanical properties and can be easily dissolved in aqueous environments.[38] According to previous reports, scaffold porosity does not change significantly after cross-linking.[39] To remove uncrosslinked glutaraldehyde residues, phosphate buffer solution was used to rinse the scaffolds. To ensure the removal of any residual chemicals, scaffolds were immersed in chilled PBS solution which was changed every hour, for the first 4 h, and then immersed in PBS solution for 20 h more at 4 °C, in comparison with other studies, where the samples were rinsed twice or thrice.[40−42] To improve the biocompatibility of the scaffolds, the concentration of GA was lowered, and the scaffolds were rinsed four times in total and kept incubated for 24 h, since in other studies the samples were cross-linked with higher concentrations under higher temperatures, resulting in a higher risk of cytotoxicity,[43] or GE/HA scaffolds were rinsed less than four times in total and not incubated in PBS. The purpose of this section is to investigate the swelling behavior of scaffolds cross-linked with different concentrations of glutaraldehyde.

Figure 4 shows the swelling ratio of scaffolds decreasing with increasing concentrations of the cross-linking agent GA. The least stable scaffolds cross-linked by 1% GA had the highest swelling property within 24 h. However, the structures of scaffolds with 1% cross-linker collapsed and dissolved after 1440 min. The structures for 5 and 10% GA cross-linked scaffolds were stable after 1440 min. Scaffolds with 10% cross-linker had the lowest water absorption, with a swelling ratio of approximately 20% after 1440 min. This compares with scaffolds cross-linked with 5% GA where the swelling ratio is 24%, a 4% increase compared to 10% GA. Thus, the higher GA concentration produces a lower swelling ratio. This is due to the different cross-linking efficiencies of different GA concentrations. It was reported previously[33] that higher cross-linker concentrations could dramatically enhance the cross-link efficiency.

Water is attracted to the hydrophilic un-cross-linked amino groups, which leads to a greater solvent volume fraction within the scaffolds. As cross-linking of gelatin can be explained by the reaction between the aldehyde functional groups and free ε-amino groups (−NH$_2$) of lysine and hydroxylysine,[44] hydrophilicity is decreased with increasing the concentrations of cross-linker, as the nucleophilic addition of the ε-NH$_2$ groups to the carbonyl groups (C═O) of the aldehyde forms a
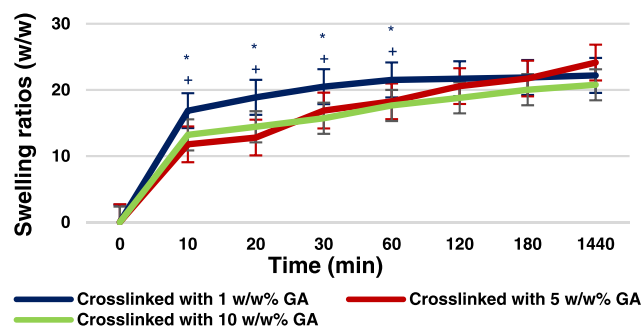
Figure 4. Effect of different cross-link concentrations, 1, 5, and 10% GA, on water uptake capability of GE scaffolds. Each measurement was repeated for five times and values were expressed in mean ± standard error of the mean. Two-way ANOVA was carried out followed by post hoc Tukey multiple comparison tests. GE solutions (5 wt %) with three different glutaraldehyde ratios were compared and values are represented statistically when *$p < 0.05$ in comparison with cross-linked 5 w/w % GA and +$p < 0.05$ when compared with cross-linked 10 w/w % GA. Statistical analysis was performed using the GraphPad Prism 6.0 software (GraphPad Software, Inc., San Diego, CA).

carbinolamine in a condensation reaction.[44] Thus, 10% GA cross-linked scaffolds had the lowest swelling ratio and water uptake ability as more amino groups were cross-linked under 10% GA compared with 1 and 5% GA resulting in greater loss of hydrophilic groups. Therefore, 5% GA was used to cross-link 5 w/w % GE scaffolds in subsequent degradation and antibacterial expriments, since these scaffolds have a good balance between high absorbency and good structural stability which are the two main desirable factors for cell adhesion and growth.[1]

Figure 5 indicates the swelling ratios as a function of time for GE/HA scaffolds compared to GE scaffolds of the same GE
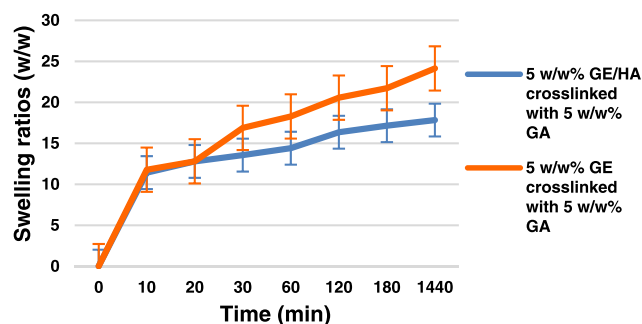

Figure 5. Comparison of the water uptake capability between GE scaffolds and GE/HA scaffolds over time, under incubation in PBS solution.

concentration (5 w/w %) and cross-linked with the same GA concentration (5 w/w %, data taken from Figure 4 for comparison). The swelling ratios increased significantly with a steep gradient within the initial 10 min, and then an increase with a smaller gradient up to 1440 min for both scaffolds. The swelling ratios for GE and GE/HA scaffolds were almost identical in the first 10 min since rapid swelling is a result of the un-cross-linked hydrophilic amino groups remaining inside both GE and GE/HA scaffolds. The high porosity of both scaffolds permits rapid infiltration of the PBS solution into the scaffolds.[45] GE and GE/HA scaffolds display a less-steep increasing gradient after the first 10 min as they approach

hydrodynamic equilibrium. This indicates that after the first 10 min, as hydration of the GE/HA matrix approaches saturation, the scaffold starts to absorb less water.[45] The swelling ratio is almost 1.3 times lower with the presence of HA in the scaffolds, compounding the effect of GA cross-linking on HA, as shown in Figure 5. This is due to the cross-linking reaction between GA and hydroxyl (−OH) groups of HA leading to a reduction in the hydrophilicity of HA, resulting in a decrease of the swelling ratio of GE/HA scaffolds in comparison to the GE scaffolds.[46] Despite this, the GE/HA scaffolds appear to have retained some good swelling capabilities of ~18% after 1440 min.

In Vitro Degradation. The resistance to hydrolytic degradation of GE and GE/HA scaffolds treated with 5 w/w % of GA is shown in Figure 6, which demonstrates the weight
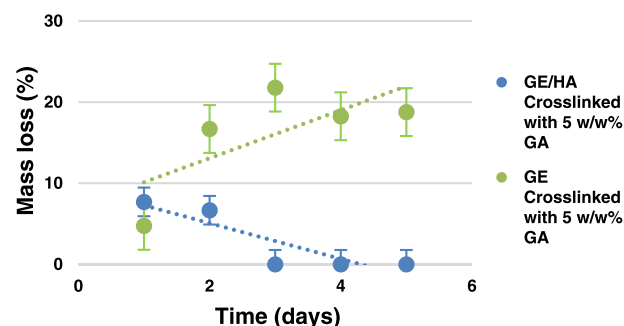

Figure 6. Comparison of mass loss between GE scaffolds and GE/HA scaffolds over time, under incubation in PBS solution at 37 °C.

loss of scaffolds as a function of incubation time in PBS at 37 °C (pH 7.4). The mass loss is associated with protein dissolution into the surrounding PBS aqueous solution.[39] The data for GE scaffolds prior to cross-linking was not included as it dissolved completely in PBS within the first hour of incubation. This is due to the lower resistance of un-cross-linked scaffolds to hydrolytic degradation.[47] Hence, cross-linking has an impact on the scaffold binding capability and degradation kinetics due to the formation of intermolecular bonds. Compared to un-cross-linked scaffolds, in vitro degradation tests demonstrate that GA cross-linking can effectively improve the stability of the scaffolds. Here, Figure 6 shows the comparison of mass loss between GE scaffolds and GE/HA scaffolds over time, under incubation in PBS solution at 37 °C.

Figure 6 indicates that the rate of degradation in HA-containing scaffolds decreased with the presence of HA content. GE/HA scaffolds showed a weight loss of 8% after 1 day, whereas GE scaffolds displayed a weight loss of 21% after 3 days. This is due to the difference in the extent of cross-linking within the different scaffolds which results in different hydrophilicity. GE/HA scaffolds had stronger intermolecular bonds and correspondingly lower hydrophilicity. The increase in the weight loss of GE scaffolds was due to greater water absorption, as the hydrophilic surface of GE enhances infiltration of water into the polymer matrix, leading to a higher rate of protein dissolution into the surrounding liquid, therefore increasing the scaffolds' degradation.[48] However, the cross-linking reaction reduces the hydrophilicity of GE/HA scaffolds, which results in a decrease in the water absorption and therefore a decrease in the rate of degradation.[46] Data were expressed as mean ± SD ($n = 3$). The apparent reversal

of mass loss after 1 day for GE/HA scaffolds can be explained by the possibility that water penetration has not reached the core of the scaffold on account of the reduced hydrophilicity relative to GE scaffolds. As a result, during drying, water from only the periphery is removed, and mass loss is observed via protein dissolution from the periphery. After immersion for >3 days, however, the time is sufficient to allow water to diffuse into the core of the scaffold. In this scenario, it is likely that 24 h of desiccation is insufficient to fully remove water from the core of the scaffold leading to an apparent reduction in the mass loss. This appears to be mirrored in the GE scenario albeit with a delay, with the apparent decrease occurring after 4 days. Due to its resistance to rapid degradation, GE/HA scaffolds were loaded with lactoferrin and assessed for antibacterial properties.

Antibacterial Activity. The materials that were used in this study to fabricate the scaffolds are biodegradable natural polymers and are derivatives of proteins found naturally in the ECM. For this reason, they have been used in the fabrication of scaffolds for tissue engineering using different techniques. It is well known that different bacterial adhesins can recognize several elements of host−cell surfaces, such as components of the extracellular matrix, including collagens, laminins, elastin, proteoglycans, and hyaluronic acid,[49] resulting in bacterial adhesion. In this case, the bacterial adhesion in scaffolds can be promoted as the size of bacteria (0.5 μm)[50] allows their infiltration and attachment on to the large pores of the scaffolds.[39] For this reason, antibacterial properties are highly desired for scaffolds, and this was a major aim of this study.

The inclusion of HA into GE scaffolds (GE/HA) results in a reduction of bacteria growth by almost 35%, in comparison with the GE scaffolds, which do not show any antibacterial activity. Antibacterial activity was evident despite the low concentration (2.5 mg/mL) of HA in comparison with other reported values in the literature.[18,21]

To further decrease the bacterial growth, GE/HA scaffolds were immersed, after their preparation, in lactoferrin (LF) solution for 3 h. LF was chosen for its antiviral, antibacterial, antiparasitic, and antifungal properties.[21,51]

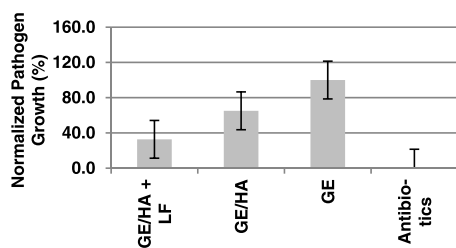Figure 7 shows the growth inhibition, which was determined by measuring the absorbance of the supernatant at 600 nm,

Figure 7. Antibacterial behavior of different scaffolds when cultured with *S. aureus* ($p < 0.05$).

after its incubation in media at 37 °C overnight. Figure 7 shows a reduction in bacterial growth of 35% for GE/HA scaffolds and 70% for GE/HA scaffolds loaded with LF ($p < 0.05$) in comparison with GE scaffolds. As GE/HA scaffolds have a good water uptake capability, scaffolds absorbed lactoferrin (LF) solution after being immersed, resulting in a further decrease of the bacterial growth. This demonstrates the feasibility of producing scaffolds with antibacterial activity from monodispersed microbubbles manufactured using a T-Junction microfluidic device.

CONCLUSIONS

A microfluidic single T-junction has been adopted to produce monodispersed microbubbles. Subsequently, stable GE/HA scaffolds were obtained by drying microbubbles with the aid of GA cross-linking. Stable and well-structured microbubbles could be produced by keeping solutions at 40 °C during processing. Scaffolds cross-linked with 5% GA solution showed good water absorption which could be used to prevent the loss of body fluid and nutrients from scaffolds during culturing in vitro and implanting in vivo. The incorporation of HA decreases the absorptive capabilities of the scaffold (which are still significant at 18%) and lowers the rate of degradation. The antibacterial properties of GE/HA scaffolds were capable of reducing bacterial growth despite a low concentration of 2.5 mg/mL. Antibacterial activity can be improved by immersing the GE/HA scaffolds in LF solution. The GE/HA scaffolds combine the advantages of gelatin and HA (e.g., good water uptake capability, biodegradable, ECM constituents) and may be a suitable candidate for use in wound-healing patches, soft tissue engineering, or as coatings for implanted medical devices.

Microbubbles offer a simple robust and inexpensive method for scaffold fabrication. The present work could provide the experimental basis for further cell growth and in vivo studies on GE/HA microbubble scaffolds using microfluidics.

EXPERIMENTAL MATERIALS AND METHODS

Materials. Gelatin (Type B, bovine skin, approx 225 g Bloom), HA (sodium salt, $(1.5-1.8) \times 10^6$ Da), Lactoferrin (bovine milk, 87×10^3 Da), and Glutaraldehyde (Grade II, 25% in H_2O, 100.12 Da) were purchased from Sigma-Aldrich Co. All of the materials and reagents were used without further purification.

Solution Preparation. GE solution, 5% (w/w), was prepared by dissolving gelatin in deionized water at 40, 50, or 60 °C with a magnetic stirrer for 1 h. The solution was heated with a temperature controller (Warner Instruments, model TC-124A) during microbubble generation to prevent gelation. GE/HA was prepared by mixing the GE with 25 mg of HA in 10 mL of deionized water, stirring for 1 h at 40 °C under the same conditions as GE. LF solution was prepared by dissolving 1 mg/mL in deionized water at room temperature (20 °C) stirring for 15 min.

Microbubble Scaffold Fabrication. The experiments for microbubble generation were performed in a T-junction microfluidic device made of poly(dimethylsiloxane). Two Teflon fluorinated ethylene polypropylene microchannels, 200 μm in diameter, were used perpendicularly to each other for the continuous phase (liquid flow) and the dispersed phase (gas flow). For the continuous phase and the dispersed phase, liquid solutions of GE, GE/HA, and N_2 gas were used. The confluence junction of the two phases penetrated into a third microchannel with 200 μm diameter, a microbubble begins to grow, as the gas pressure and the flow in the main channel distort the bubble in the downstream direction, shown in Figure 8.

Breakup of the gas−liquid streams is dominated by the pressure drop across the bubble as it forms. The aqueous solutions are loaded into a syringe and placed in the syringe
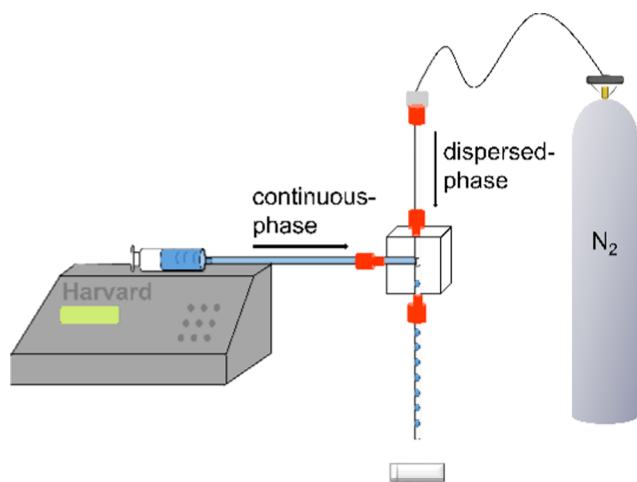
Figure 8. Schematic representation of the process of bubble generation in a T-junction cross-flow microfluidic device setup.

pump (Harvard Apparatus Ltd., Edenbridge U.K.), which delivers the solution to the microchannel. At the same time, N_2 gas was passed through the other microchannel resulting in microbubble formation. Monodispersed microbubbles spontaneously self-assembled into liquid foam structures and after leaving them to dry, were solidified.[52] During the drying process, due to the pressure difference between the bubbles and the ambient atmosphere, the film of the bubbles bursts, leaving only the plateau borders, resulting in structure creation. By collecting the microbubbles on a glass slide enable forming of multiple layers of the microbubbles. By collecting the microbubbles on a glass slide, 3D scaffolds were formed from the multiple layers of the microbubbles. GE scaffolds were cross-linked with 1, 5, and 10% concentrations of GA solution. GE/HA scaffolds were cross-linked with 5% of GA. The cross-linked GE and GE/HA scaffolds were then immersed in PBS solution at 4 °C for 24 h to completely remove any residues of GA. GE/HA scaffolds were later immersed in lactoferrin (LF) solution to load them with LF.

Stability Study. GE (5 w/w %) was chosen as the continuous phase to generate microbubbles. Three GE solutions were made by dissolving 5 w/w % gelatin in deionized water at temperatures of 40, 50, and 60 °C, separately. Material characterization was carried out at room temperature. The mean diameter of microbubbles produced at various gas pressures and flow rates was measured as a function of time. For each sample, 100 microbubbles were chosen stochastically and measured every 2 min until all of the microbubbles burst or their GE shell dried. The effect of the temperature on the stability, structure, and size of microbubble was studied.

Visualization and Analysis. Scaffolds were observed under an optical microscope (Zeiss Axiotech, Germany) fitted with a camera (Nikon Eclipse ME 600, Japan) at a magnification of 5×. A high-speed Phantom v5.0 camera with a maximum resolution of 800 × 600 pixels at up to 4800 fps with a recording time of 1.2 s was used to record live microbubble formation videos (see Supporting Information). The bubble-formation processes were analyzed under different flow rate ratio conditions. The size and structure of microbubbles were captured using the same microscope. Measuring the diameter of at least 100 microbubbles per sample by using Image J software, we were able to calculate the

average bubble diameter (dav) and the polydispersity index (σ). Polydispersity index is defined by the following equation

$$\sigma = \delta/\text{dav} \times 100\% \tag{1}$$

where δ is the standard deviation.

Cross-Linking of Scaffolds. Three different cross-linker solutions of 1, 5, and 10 w/w % concentrations of GA were prepared in 10 mL of deionized water. Cross-linker concentrations of GA (1, 5, and 10 w/w %) were applied on scaffolds. The samples were dried in ambient conditions for 24 h. Scaffolds were then rinsed with PBS every 1 h for the first 4 h and then immersed in PBS for a further 20 h at 4 °C to remove residual GA.

Characterization of Scaffolds. The swelling ratio allows us to determine the capacity of the hydrogel to imbibe large amounts of water.[53] GE scaffolds were cross-linked with a 1, 5, or 10% solution of GA. The scaffolds were then dried and weighed (W_d). Scaffolds were then immersed in phosphate-buffered saline (PBS, pH 7.4) for 24 h at 37 °C. The wet weight (W_t) of the samples was measured after 10, 20, 30, 60, 120, 180, and 1440 min. Swelling ratio was calculated using the eq 2

$$\text{SR} = (W_t - W_d)/W_d \times 100\% \tag{2}$$

where SR is the swelling ratio (%) and is defined[1] as the ratio of the weight increase ($W_t - W_d$) to the initial dry weight (W_d).

In vitro degradation of scaffolds was investigated by measuring weight loss over time under static culture conditions. The weight loss was calculated from the difference between the weight of samples at the start of experiment and the residual weight after immersing samples in PBS solution for a period of 5 days.[49] Experiments were performed in PBS buffer at 37 °C every day for 5 days to mimic a biological environment. Then, scaffolds were taken out of solutions daily and placed in a desiccator to dry for 24 h before residual weight measurement (W_r). The extent of the in vitro degradation was calculated as the percentage of weight loss before and after PBS treatment[1] using the equation given

$$W_l = (W_0 - W_r)/W_0 \times 100\% \tag{3}$$

where W_l is the percentage of weight loss, W_0 is the weight of scaffolds at the start of experiment, and W_r is the sample weight after desiccator drying. Degradation tests have been defined as the degradation involving backbone chain breakage and a diminution in average molecular weight.[54] Here, the degradation test helps us understand how facilely the scaffold can be degraded over time.

The experiments for swell ratio and degradation were conducted three times, and all values were reported as the mean and standard deviation.

Antibacterial Assay. S. aureus (ATCC 25923) was used to check the antibacterial properties of the samples. Bacterial strain was cultured aerobically at 37 °C in a Tryptic Soy Broth (TSB) medium at pH 7.4. One colony was transferred to 10 mL of TSB medium and incubated at 37 °C for 20 h. To obtain bacteria in the mid logarithmic phase growth, the absorbance (600 nm) of overnight culture was adjusted to 0.00022, corresponding to a final density of 105 CFU/mL. Scaffolds were placed into a 96-well plate and sterilized using UVGI for 15 min. After the sterilization, 180 μL of S. aureus, A_{600} = 0.00022, was added to each well and incubated for 24 h at 37 °C. For the negative control, gelatin scaffolds were

incubated with *S. aureus* using the same method. For the positive control, penicillin streptomycin (Pen Strep) was added. To check the bacterial growth or inhibition after 24 h, the absorbance of the supernatant at 600 nm was measured.

■ ASSOCIATED CONTENT

Ⓢ Supporting Information

The Supporting Information is available free of charge on the ACS Publications website at DOI: 10.1021/acsomega.8b02573.

    Generation of microbubbles using a microfluidic T-junction device (ZIP)

■ AUTHOR INFORMATION

Corresponding Author

*E-mail: m.edirisinghe@ucl.ac.uk.

ORCID Ⓘ

Mohan Edirisinghe: 0000-0001-8258-7914

Author Contributions

C.K. and X.J. designed the experiments. X.J. and M.E. supervised the experiments. C.K., X.J., and W.K.L. performed experiments. C.K. analyzed and interpreted data. C.K. manufactured materials. C.K. and X.J. wrote the manuscript. All authors revised and corrected the final manuscript.

Notes

The authors declare no competing financial interest.

■ ACKNOWLEDGMENTS

■ REFERENCES

(1) Zhang, F.; He, C.; Cao, L.; Feng, W.; Wang, H.; Mo, X.; Wang, J. Fabrication of gelatin–hyaluronic acid hybrid scaffolds with tunable porous structures for soft tissue engineering. *Int. J. Biol. Macromol.* **2011**, *48*, 474–481.

(2) Lian, Y.; Yuan, L.; Ji, L.; Zhang, K. Gelatin/hyaluronic acid nanofibrous scaffolds: biomimetics of extracellular matrix. *Acta Biochim. Biophys. Sin.* **2013**, *45*, 700–703.

(3) Kim, T. G.; Chung, H. J.; Park, T. G. Macroporous and nanofibrous hyaluronic acid/collagen hybrid scaffold fabricated by concurrent electrospinning and deposition/leaching of salt particles. *Acta Biomater.* **2008**, *4*, 1611–1619.

(4) Poursamar, S. A.; Hatami, J.; Lehner, N. A.; da Silva, C. L.; Ferreira, F. C.; Antunes, A. P. M. Potential application of gelatin scaffolds prepared through in situ gas foaming in skin tissue engineering. *Int. J. Polym. Mater. Polym. Biomater.* **2016**, *65*, 315–322.

(5) Karageorgiou, V.; Kaplan, D. Porosity of 3D biomaterial scaffolds and osteogenesis. *Biomaterials* **2005**, *26*, 5474–5491.

(6) Elsayed, M.; Kothandaraman, A.; Edirisinghe, M.; Huang, J. Porous Polymeric Films from Microbubbles Generated Using a T-Junction Microfluidic Device. *Langmuir* **2016**, *32*, 13377–13385.

(7) Chung, K. Y.; Mishra, N. C.; Wang, C. C.; Lin, F. H.; Lin, K. H. Fabricating scaffolds by microfluidics. *Biomicrofluidics* **2009**, *3*, No. 022403.

(8) Jiang, X.; Zhang, Y.; Edirisinghe, M.; Parhizkar, M. Combining microfluidic devices with coarse capillaries to reduce the size of monodisperse microbubbles. *RSC Adv.* **2016**, *6*, 63568–63577.

(9) Wang, C. C.; Yang, K. C.; Lin, K. H.; Liu, H. C.; Lin, F. H. A highly organized three-dimensional alginate scaffold for cartilage tissue engineering prepared by microfluidic technology. *Biomaterials* **2011**, *32*, 7118–7126.

(10) Ekemen, Z.; Chang, H.; Ahmad, Z.; Bayram, C.; Rong, Z.; Denkbas, E. B.; Stride, E.; Vadgama, P.; Edirisinghe, M. Fabrication of Biomaterials via Controlled Protein Bubble Generation and Manipulation. *Biomacromolecules* **2011**, *12*, 4291–4300.

(11) He, C.; Xiao, G.; Jin, X.; Sun, C.; Ma, P. X. Electrodeposition on nanofibrous polymer scaffolds: Rapid mineralization, tunable calcium phosphate composition and topography. *Adv. Funct. Mater.* **2010**, *20*, 3568–3576.

(12) Tuin, A.; Zandstra, J.; Kluijtmans, S. G.; Bouwstra, J. B.; Harmsen, M. C.; Van Luyn, M. J. A. Hyaluronic acid-recombinant gelatin gels as a scaffold for soft tissue regeneration. *Eur. Cells Mater.* **2012**, *24*, 320–330.

(13) Ramsden, L.; Rider, C. C. Selective and differential binding of interleukin (IL)-1 alpha, IL-1 beta, IL-2 and IL-6 to glycosaminoglycans. *Eur. J. Immunol.* **1992**, *22*, 3027–3031.

(14) Fernandez-Botran, R.; Yan, J.; Justus, D. E. Binding of interferon gamma by glycosaminoglycans: a strategy for localization and/or inhibition of its activity. *Cytokine* **1999**, *11*, 313–325.

(15) Tsai, S. W.; Liu, R. L.; Hsu, F. Y.; Chen, C. C. A study of the influence of polysaccharides on collagen self-assembly: nanostructure and kinetics. *Biopolymers* **2006**, *83*, 381–388.

(16) Shu, X. Z.; Liu, Y.; Palumbo, F.; Prestwich, G. D. Disulfide-crosslinked hyaluronan-gelatin hydrogel films: a covalent mimic of the extracellular matrix for in vitro cell growth. *Biomaterials* **2003**, *24*, 3825–3834.

(17) Knopf-Marques, H.; Barthes, J.; Wolfova, L.; Vidal, B.; Koenig, G.; Bacharouche, J.; Francius, G.; Sadam, H.; Liivas, U.; Lavalle, P.; Vrana, N. E. Auxiliary Biomembranes as a Directional Delivery System To Control Biological Events in Cell-Laden Tissue-Engineering Scaffolds. *ACS Omega* **2017**, *2*, 918–929.

(18) Romanò, C. L.; De Vecchi, E.; Bortolin, M.; Morelli, I.; Drago, L. Hyaluronic Acid and Its Composites as a Local Antimicrobial/Antiadhesive Barrier. *J. Bone Jt. Infect.* **2017**, *2*, 63–72.

(19) Pirnazar, P.; Wolinsky, L.; Nachnani, S.; Haake, S.; Pilloni, A.; Bernard, G. W. Bacteriostatic Effects of Hyaluronic Acid. *J. Periodontol.* **1999**, *70*, 370–374.

(20) Park, Y. D.; Tirelli, N.; Hubbell, J. A. Photopolymerized hyaluronic acid-based hydrogels and interpenetrating networks. *Biomaterials* **2003**, *24*, 893–900.

(21) Jenssen, H.; Hancock, R. E. Antimicrobial properties of lactoferrin. *Biochimie* **2009**, *91*, 19–29.

(22) Kim, S. E.; Yun, Y. P.; Shim, K. S.; Park, K.; Choi, S. W.; Suh, D. H. Effect of lactoferrin-impregnated porous poly(lactide-co-glycolide) (PLGA) microspheres on osteogenic differentiation of rabbit adipose-derived stem cells (rADSCs). *Colloids Surf., B* **2014**, *122*, 457–464.

(23) Diarra, M. S.; Petitclerc, D.; Deschênes, E.; Lessard, N.; Grondin, G.; Talbot, B. G.; Lacasse, P. Lactoferrin against *Staphylococcus aureus* Mastitis Lactoferrin alone or in combination with penicillin G on bovine polymorphonuclear function and mammary epithelial cells colonisation by *Staphylococcus aureus*. *Vet. Immunol. Immunopathol.* **2003**, *95*, 33–42.

(24) Iigo, M.; Kuhara, T.; Ushida, Y.; Sekine, K.; Moore, M. A.; Tsuda, H. Inhibitory effects of bovine lactoferrin on intestinal polyposis in the ApcMin mouse. *Cancer Lett.* **1998**, *17*, 35–40.

(25) Zhang, Y.; Lima, C. F.; Rodrigues, L. R. Anticancer effects of lactoferrin: underlying mechanisms and future trends in cancer therapy. *Nutr. Rev.* **2014**, *72*, 763–773.

(26) Guillen, C.; McInnes, I. B.; Vaughan, D.; Speekenbrink, A. B.; Brock, J. H. The effects of local administration of lactoferrin on inflammation in murine autoimmune and infectious arthritis. *Arthritis Rheum.* **2000**, *43*, 2073–2080.

(27) Kuehnert, M. J.; Hill, H. A.; Kupronis, B. A.; Tokars, J. I.; Solomon, S. L.; Jernigan, D. B. Methicillin-resistant–*Staphylococcus aureus* Hospitalizations, United States. *Emerging Infect. Dis.* **2005**, *11*, 868–872.

(28) Klein, E.; Smith, D. L.; Laxminarayan, R. Hospitalizations and Deaths Caused by Methicillin-Resistant *Staphylococcus aureus*, United States, 1999–2005. *Emerging Infect. Dis.* **2007**, *13*, 1840–1846.

(29) Murphy, C. M.; Haugh, M. G.; O'Brien, F. J. The effect of mean pore size on cell attachment, proliferation and migration in collagen–

glycosaminoglycan scaffolds for bone tissue engineering. *Biomaterials* **2010**, *31*, 461−466.

(30) De la Ossa, J. G.; Trombi, L.; D'Alessandro, D.; Coltelli, M. B.; Pio Serino, L.; Pini, R.; Lazzeri, A.; Petrini, M.; Danti, S. Pore Size Distribution and Blend Composition Affect In Vitro Prevascularized Bone Matrix Formation on Poly(Vinyl Alcohol)/Gelatin Sponges. *Macromol. Mater. Eng.* **2017**, *302*, No. 1700300.

(31) Gultekinoglu, M.; Jiang, X.; Bayram, C.; Ulubayram, K.; Edirisinghe, M. Honeycomb-like PLGA-b-PEG Structure Creation with T-Junction Microdroplets. *Langmuir* **2018**, *34*, 7989−7997.

(32) Beneventi, D.; Carre, B.; Gandini, A. Role of surfactant structure on surface and foaming properties. *Colloids Surf., A* **2001**, *189*, 65−73.

(33) Gerber, F.; Krafft, M. P.; Waton, G.; Vandamme, T. F. Microbubbles with exceptionally long life-synergy between shell and internal phase components. *New J. Chem.* **2006**, *30*, 524−527.

(34) Liu, H.; Zhang, Y. Droplet formation in a T-shaped microfluidic junction. *J. Appl. Phys.* **2009**, *106*, No. 034906.

(35) Yasuno, M.; Sugiura, S.; Iwamoto, S.; Nakajima, M.; Shono, A.; Satoh, K. Monodispersed microbubble formation using microchannel technique. *AIChE J.* **2004**, *50*, 3227.

(36) Zhang, W. Evaluation of effect of viscosity changes on bubble size in a mechanical flotation cell. *Trans. Nonferrous Met. Soc. China* **2014**, *24*, 2964−2968.

(37) Xu, J. H.; Li, S. W.; Chen, G. G.; Luo, G. S. Formation of monodisperse microbubbles in a microfluidic device. *AIChE J.* **2006**, *52*, 2254−2259.

(38) Yazdimamaghani, M.; Vashaee, D.; Assefa, S.; Walker, K. J.; Madihally, S. V.; Köhler, G. A.; Tayebi, L. Hybrid Macroporous Gelatin/Bioactive-Glass/Nanosilver Scaffolds with Controlled Degradation Behavior and antimicrobial activity for bone tissue engineering. *J. Biomed. Nanotechnol.* **2014**, *10*, 911−931.

(39) Grover, C. N.; Cameron, R. E.; Best, S. M. Investigating the morphological, mechanical and degradation properties of scaffolds comprising collagen, gelatin and elastin for use in soft tissue engineering. *J. Mech. Behav. Biomed. Mater.* **2012**, *10*, 62−74.

(40) Wu, X.; Liu, Y.; Li, X.; Wen, P.; Zhang, Y.; Long, Y.; Wang, X.; Guo, Y.; Xing, F.; Gao, J. Preparation of aligned porous gelatin scaffolds by unidirectional freeze-drying method. *Acta Biomater.* **2010**, *6*, 1167−1177.

(41) Zhang, F.; He, C.; Cao, L.; Feng, W.; Wang, H.; Mo, X.; Wang, J. Fabrication of gelatin−hyaluronic acid hybrid scaffolds with tunable porous structures for soft tissue engineering. *Int. J. Biol. Macromol.* **2011**, *48*, 474−481.

(42) Zhou, Z.; Yang, Z.; Huang, T.; Liu, L.; Liu, Q.; Zhao, Y.; Zeng, W.; Yi, Q.; Cao, D. Effect of Chemical Cross-linking on Properties of Gelatin/Hyaluronic Acid Composite Hydrogels. *Polym.-Plast. Technol. Eng.* **2013**, *52*, 45−50.

(43) Bigi, A.; Cojazzi, G.; Panzavolta, S.; Rubini, K.; Roveri, N. Mechanical and thermal properties of gelatin films at different degrees of glutaraldehyde crosslinking. *Biomaterials* **2001**, *22*, 763−768.

(44) Farris, S.; Song, J.; Huang, Q. Alternative Reaction Mechanism for the Cross-Linking of Gelatin with Glutaraldehyde. *J. Agric. Food Chem.* **2010**, *58*, 998−1003.

(45) Shull, C. A.; Shull, S. P. Absorption of Moisture by Gelatin in a Saturated Atmosphere. *Am. J. Bot.* **1920**, *7*, 318−326.

(46) Tomihata, K.; Ikada, Y. Crosslinking of Hyaluronic Acid with Glutaraldehyde. *J. Polym. Sci., Part A: Polym. Chem.* **1997**, *35*, 3553−3559.

(47) Park, S. N.; Park, J. C.; Kim, H. O.; Song, M. J.; Suh, H. Characterization of porous collagen/hyaluronic acid scaffold modified by 1-ethyl-3-(3-dimethylaminopropyl)carbodiimide cross-linking. *Biomaterials* **2002**, *23*, 1205−1212.

(48) Saadat, A.; Karbasi, S.; Behnam Ghader, A. A.; Khodaei, M. Characterization of Biodegradable P3HB/HA Nanocomposite Scaffold for Bone Tissue Engineering. *Procedia Mater. Sci.* **2015**, *11*, 217−223.

(49) Pizarro-Cerdá, J.; Cossart, P. Bacterial Adhesion and Entry into Host Cells. *Cell* **2006**, *124*, 715−727.

(50) Mi, F. L.; Shyu, S. S.; Wu, Y. B.; Lee, S. T.; Shyong, J. Y.; Huang, R. N. Fabrication and characterization of a sponge-like asymmetric chitosan membrane as a wound dressing. *Biomaterials* **2001**, *22*, 165−173.

(51) Görmez, U.; Kürkcü, M.; Benlidayi, M. E.; Ulubayram, K.; Sertdemir, Y.; Dağlioğlu, K. Effects of bovine lactoferrin in surgically created bone defects on bone regeneration around implants. *J. Oral Sci.* **2015**, *57*, 7−15.

(52) Parhizkar, M.; Sofokleous, P.; Stride, E.; Edirisinghe, M. Novel preparation of controlled porosity particle/fibre loaded scaffolds using a hybrid micro-fluidic and electrohydrodynamic technique. *Biofabrication* **2014**, *6*, No. 045010.

(53) Park, H.; Guo, X.; Temenoff, J. S.; Tabata, Y.; Caplan, A. I.; Kasper, F. K.; Mikos, A. G. Effect of Swelling Ratio of Injectable Hydrogel Composites on Chondrogenic Differentiation of Encapsulated Rabbit Marrow Mesenchymal Stem Cells In Vitro. *Biomacromolecules* **2009**, *10*, 541−546.

(54) Ratner, B. D.; Gladhill, K. W.; Horbett, T. A. Analysis of in vitro enzymatic and oxidative. *J. Biomed. Mater. Res.* **1988**, *22*, 509−527.